The Astrophysical Journal, 717:209–222, 2010 July 1 doi:10.1088/0004-637X/717/1/209

A RUNAWAY BLACK HOLE IN COSMOS: GRAVITATIONAL WAVE OR SLINGSHOT RECOIL?

F. Civano[1], M. Elvis[1], G. Lanzuisi[1,2], K. Jahnke[3], G. Zamorani[4], L. Blecha[5], A. Bongiorno[6], M. Brusa[6], A. Comastri[4], H. Hao[1], A. Leauthaud[7], A. Loeb[5], V. Mainieri[8], E. Piconcelli[9], M. Salvato[10], N. Scoville[10], J. Trump[11], C. Vignali[12], T. Aldcroft[1], M. Bolzonella[4], E. Bressert[1], A. Finoguenov[6,13], A. Fruscione[1], A. M. Koekemoer[14], N. Cappelluti[6], F. Fiore[9], S. Giodini[6], R. Gilli[4], C. D. Impey[11], S. J. Lilly[15], E. Lusso[4,12], S. Puccetti[16], J. D. Silverman[15], H. Aussel[17], P. Capak[10], D. Frayer[10], E. Le Floc'h[18], H. J. McCracken[19], D. B. Sanders[18], D. Schiminovich[20], and Y. Taniguchi[21]
[1] Harvard Smithsonian Center for Astrophysics, 60 Garden Street, Cambridge, MA 02138, USA
[2] Dipartimento di Fisica, Università di Roma La Sapienza, P. le A. Moro 2, 00185 Roma, Italy
[3] Max Planck Institut für Astronomie, Königstuhl 17, Heidelberg, D-69117, Germany
[4] INAF-Osservatorio Astronomico di Bologna, via Ranzani 1, I-40127 Bologna, Italy
[5] Astronomy Department, Harvard University, 60 Garden Street, Cambridge, MA 02138, USA
[6] Max Planck Institut für Extraterrestrische Physik Giessenbachstrasse 1, D–85748 Garching, Germany
[7] LBNL & BCCP, University of California, Berkeley, CA 94720, USA
[8] European Southern Observatory, Karl-Schwarzschild-Str. 2, D-85748 Garching, Germany
[9] INAF-Osservatorio Astronomico di Roma, via di Frascati 33, I-00040 Monteporzio Catone, Italy
[10] California Institute of Technology, MC 105-24, 1200 East California Boulevard, Pasadena, CA 91125, USA
[11] Steward Observatory, University of Arizona, 933 North Cherry Avenue, Tucson, AZ 85721, USA
[12] Dipartimento di Astronomia, Università degli Studi di Bologna, Via Ranzani 1, I-40127 Bologna, Italy
[13] University of Maryland, Baltimore County, 1000 Hilltop Circle, Baltimore, MD 21250, USA
[14] Space Telescope Science Institute, 3700 San Martin Drive, Baltimore, MD 21218, USA
[15] Institute of Astronomy, Swiss Federal Institute of Technology (ETH Hönggerberg), CH-8093, Zürich, Switzerland
[16] ASI Science Data Center, via Galileo Galilei, 00044 Frascati, Italy
[17] AIM Unité Mixte de Recherche CEA CNRS, Université Paris VII UMR n158, Paris, France
[18] Institute for Astronomy, University of Hawaii, 2680 Woodlawn Drive, Honolulu, HI 96822, USA
[19] Institut d'Astrophysique de Paris, UMR 7095 CNRS, Université Pierre et Marie Curie, 98 bis Boulevard Arago, F-75014 Paris, France
[20] Department of Astronomy, Columbia University, MC2457, 550 West 120 Street New York, NY 10027, USA
[21] Research Center for Space and Cosmic Evolution, Ehime University, Bunkyo-cho, Matsuyama 790-8577, Japan
Received 2009 August 3; accepted 2010 May 9; published 2010 June 9

ABSTRACT

We present a detailed study of a peculiar source detected in the COSMOS survey at $z = 0.359$. Source CXOC J100043.1+020637, also known as CID-42, has two compact optical sources embedded in the same galaxy. The distance between the two, measured in the *HST*/ACS image, is $0\farcs495 \pm 0\farcs005$ that, at the redshift of the source, corresponds to a projected separation of 2.46 ± 0.02 kpc. A large ($\sim$1200 km s^{-1}) velocity offset between the narrow and broad components of Hβ has been measured in three different optical spectra from the VLT/VIMOS and Magellan/IMACS instruments. CID-42 is also the only X-ray source in COSMOS, having in its X-ray spectra a strong *redshifted* broad absorption iron line and an iron emission line, drawing an *inverted* P-Cygni profile. The *Chandra* and *XMM-Newton* data show that the absorption line is variable in energy by $\Delta E = 500$ eV over four years and that the absorber has to be highly ionized in order not to leave a signature in the soft X-ray spectrum. That these features—the morphology, the velocity offset, and the *inverted* P-Cygni profile—occur in the same source is unlikely to be a coincidence. We envisage two possible explanations, both exceptional, for this system: (1) a gravitational wave (GW) recoiling black hole (BH), caught 1–10 Myr after merging; or (2) a Type 1/Type 2 system in the same galaxy where the Type 1 is recoiling due to the slingshot effect produced by a triple BH system. The first possibility gives us a candidate GW recoiling BH with both spectroscopic and imaging signatures. In the second case, the X-ray absorption line can be explained as a BAL-like outflow from the foreground nucleus (a Type 2 AGN) at the rearer one (a Type 1 AGN), which illuminates the otherwise undetectable wind, giving us the first opportunity to show that fast winds are present in obscured active galactic nuclei (AGNs), and possibly universal in AGNs.

Key words: galaxies: active – galaxies: formation – galaxies: interactions – galaxies: nuclei – quasars: absorption lines

Online-only material: color figures

1. INTRODUCTION

Double super-massive black holes (SMBHs) within a single galaxy are predicted from the combination of hierarchical models of structure formation (see Colpi & Dotti 2009 for a recent review), and the observed link between black hole (BH) mass and host galaxy bulge mass in the local universe (e.g., Magorrian et al. 1998; Gebhardt 2000). Kiloparsec-scale double nuclei should be common at redshift $z \sim 2$ where the merging process is very efficient (Springel et al. 2005), but at this high z they are hard to resolve. At later epochs ($z < 0.7$), they are easier to find but the merger rate is lower (Hopkins et al. 2008) and binary SMBHs should be relatively scarce. For these reasons, observational evidence for binary active SMBHs at kiloparsec separations remains sparse. A few low-redshift examples have been found. The most famous double active SMBHs are the highly obscured pair in the ultra-luminous infrared galaxy (ULIRG) NGC 6240 (Komossa et al. 2003; $z = 0.0245$). *Chandra* imaging and spectroscopy of NGC 6240 show the presence of two active galactic nuclei (AGNs) separated by just

1.2 kpc. Only few other AGN pairs at kiloparsec separations have been discovered so far, all by chance: Arp 299 (Ballo et al. 2004; $z = 0.01$), Mrk 463 (Bianchi et al. 2008; $z = 0.05$), 3C 75 (Hudson et al. 2006; $z = 0.02$), and 0402+379 (Rodriguez et al. 2006; $z = 0.05$). A candidate sub-parsec binary system at $z = 0.38$ has been recently discovered in the Sloan Digital Sky Survey (SDSS) through the detection of two emission-line systems in the optical spectrum (Boroson & Lauer 2009), but this interpretation is still under debate (e.g., Chornock et al. 2010).

Once the SMBH binary tightens, its merger is characterized by the emission of gravitational waves (GWs) and the merged BHs under favorable conditions (of galaxy mass ratio and BH spins) can recoil with respect to the center of the galaxy (Peres 1962; Bekenstein 1973) at substantial velocities (few $\times$ 10^2–10^3 km s^{-1}; Campanelli et al. 2007a). If not enough mass is driven to the SMBH binary before the merger, it can stall until the arrival of a third galaxy induces the hardening of the binary which ejects the BH that arrived for gravitational slingshot effect (Saslaw et al. 1974).

Recently, observational searches were initiated for single quasars that are spatially or spectroscopically displaced from their host galaxy due to GW recoil after the merger (e.g., Bonning et al. 2007). Only a few candidates have been reported so far (Komossa et al. 2008; Shields et al. 2009), all of them discovered through the detection of multiple line systems in optical spectra; however, more prosaic interpretations for these candidates are not yet ruled out. The quasar HE 0450-2958 is a candidate to be BH ejected by the nucleus of a companion galaxy during a major merger (Magain et al. 2005; Hoffman & Loeb 2006), but questions remain about the nature of this source (e.g., Merritt et al. 2006; Kim et al. 2007; Jahnke et al. 2009a).

A survey for binary SMBH systems or the discovery of many recoiling BHs would be helpful to test evolutionary merger models and to put more robust constraints on our understanding of BH and galaxy co-evolution (e.g., Hopkins et al. 2008).

The Cosmic Evolution Survey (COSMOS; Scoville et al. 2007a) is a deep multiwavelength survey of 2 deg^2, based on a 590 orbit Advanced Camera for Surveys (ACS) program (Koekemoer et al. 2007), the largest mosaic ever made by the *Hubble Space Telescope* (*HST*). Of the 10^6 galaxies to $i_{\rm AB} \sim 27$ detected in the full field, the *i*-band (F814W) ACS data provide morphological information down to $i_{\rm AB} < 23$ for 70,000 galaxies and enable detailed structural analysis out to $z \sim 0.8$ for ~16,000 galaxies. The large number of spectra (>20,000; Lilly et al. 2007, 2009; Trump et al. 2007) available for galaxies and quasars allows us to search for sources with more than one line system, although the typical resolution available ($R = 600$–700) only allows sources with high-velocity shifts to be found. The rich multiwavelength COSMOS database allows a detailed study of the source spectral energy distributions (SEDs) at all frequencies from radio to X-ray. These properties make COSMOS an excellent database in which to look for sources just before or after the merging of SMBH binaries. According to the prediction of Volonteri & Madau (2008), the number of detectable off-center AGNs (up to 30 kpc away from the center of its host) in the *HST* COSMOS area should be ~30, for the best case of large kicks (spinning holes), long decay timescales (no bulge), and long active phase, while considering those emitting X-ray the expected number is ~1. In contrast, the short lifetime of binary BHs at small separations implies a much lower number of sub-parsec candidates in the whole area, even at low redshift (<1/deg^2; Volonteri et al. 2009).

SMBHs are easier to find when they are active, and X-ray surveys are the most efficient means for finding AGNs (e.g., Brandt & Hasinger 2005). Hence, we started our survey for pre- and post-binary candidates with the optical counterparts of X-ray sources within COSMOS.

A visual inspection of the optical counterparts of all 2600 X-ray sources, detected in the *Chandra*–COSMOS (C-COSMOS; Elvis et al. 2009) and *XMM*–COSMOS (Hasinger et al. 2007) surveys, using the *HST*/ACS F814W images (Koekemoer et al. 2007; Leauthaud et al. 2007), led to the discovery of just one candidate recoil SMBH in the source CXOC J100043.1+020637 (CID-42; Elvis 2009) at $z = 0.359$. At the same time, Comerford et al. (2009) reported the discovery of dual AGNs spatially and spectroscopically resolved in the same source through the detection of two emission-line systems in a Keck/DEIMOS spectrum (200 s exposure time), though at a limited signal-to-noise ratio (S/N).

We report here a detailed study of CID-42, including the SED analysis and optical and X-ray imaging and spectroscopy. We discuss several models for the nature of this system.

In this paper, magnitudes are reported in the AB system (Oke & Gunn 1983) and a *WMAP* five year cosmology[22] with $H_0 = 71$ km s^{-1} Mpc^{-1}, $\Omega_M = 0.26$, and $\Omega_\Lambda = 0.74$ is assumed.

2. THE X-RAY SOURCE CXOC J100043.1+020637

The peculiar source is the optical counterpart of the X-ray source CID-42 (Elvis et al. 2009; F. Civano et al. 2010, in preparation), also known as XMMU J100043.1+020636 (Cappelluti et al. 2009; Brusa et al. 2007, 2010). Figure 1 shows a 30″ × 30″two color image, created by overlaying the *Chandra* 0.5–8 keV (in purple color scale) and ACS F814W (in yellow/white color scale) images, around CID-42. Two sources (white) are clearly visible in the *HST* image. The galaxy shows structures to the NE and SW suggestive of tidal tails formed during a first galaxy–galaxy encounter (e.g., Cox et al. 2006).

CID-42 is in the central area of the COSMOS field and, for this reason, has been observed in all the COSMOS bands, multiple times in some cases, allowing the construction of the FIR–UV SED. In Figure 2 (left panel), the total rest-frame SED (using data from Frayer et al. 2009; Le Floc'h et al. 2009; Sanders et al. 2007; Capak et al. 2007; McCracken et al. 2010; Taniguchi et al. 2007; Zamojski et al. 2007) is compared with the template of a Seyfert 1.8 and of the double nucleus prototype NGC 6240 (dashed and dotted line, respectively; Polletta et al. 2007) normalized to the *K*-band luminosity. The Elvis et al. (1994) quasar SED, normalized as will be explained in Section 3.1, is also shown (continuous red line). The radio emission is 0.138 ± 0.038 mJy at 20 cm (Schinnerer et al. 2007; Bondi et al. 2008), and the source is classified as radio-quiet using the Wilkes & Elvis (1987) definition ($R_L = \log(f_{5\,\rm GHz}/f_B) = -0.55$). Although the optical spectrum shows strong emission lines typical of an AGN (see Section 4.1), the optical SED is dominated by the galaxy component. The infrared luminosity is lower than that of NGC 6240 (normalized in the *K* band) but consistent with that of a luminous infrared galaxy ($L_{24\,\mu\rm m} \sim 3.2 \times 10^{10}\,L_\odot$) which could suggest ongoing star formation activity as expected in a merger phase (Mihos & Hernquist 1996). However, nuclear activity could be contributing strongly to the IR emission, as shown from the comparison with the

[22] http://lambda.gsfc.nasa.gov/product/map/dr3/params/lcdm_sz_lens_wmap5.cfm

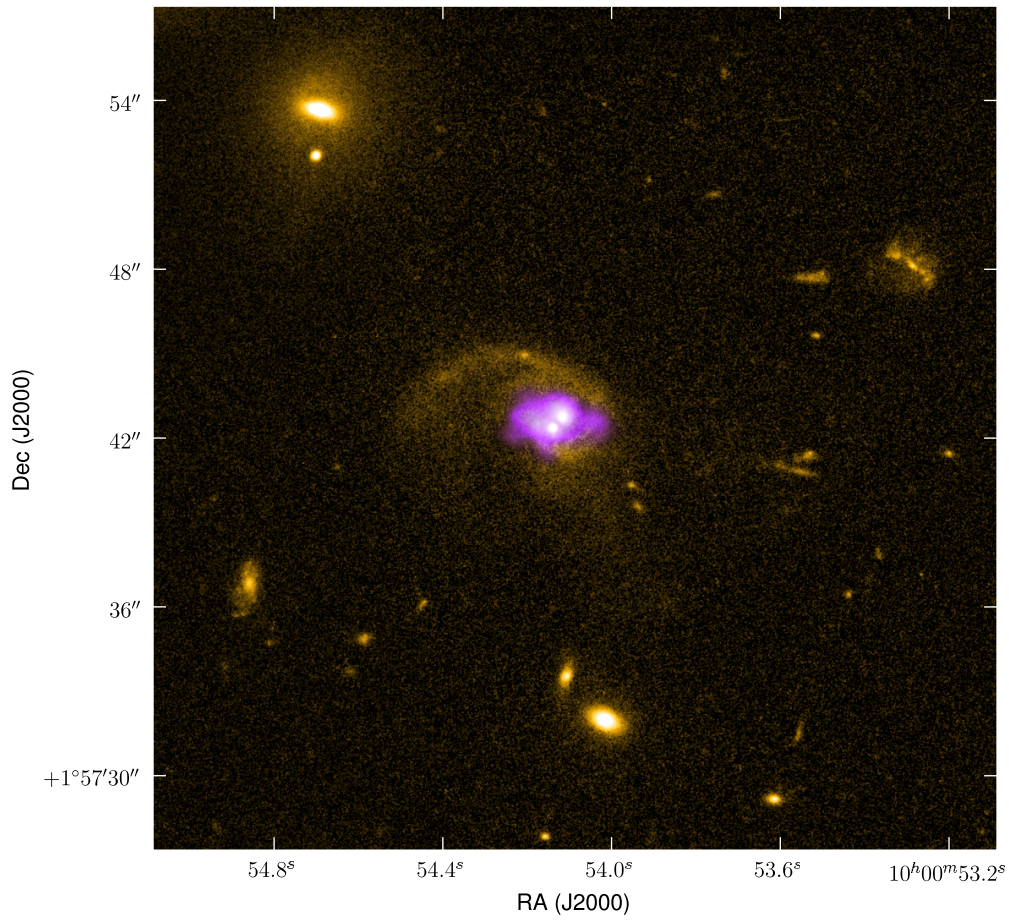

Figure 1. Two band 30″ × 30″ image of the double nucleus source. North is up, east is to the left. The image has been made summing the *Chandra* ACIS 0.5–8 keV (purple color scale) and ACS F814W (yellow/white color scale) images. The ACS data was stretched with a logarithmic function. The high resolution of the ACS image (0.″03 pixel^{-1}) allows to resolve the two sources. The X-ray data was optimized using the GREYCStoration algorithm (http://cimg.sourceforge.net/greycstoration/).

Seyfert 1.8 SED. The good fit to the UV with the last SED suggests that the obscuring gas is not Compton thick as in NGC 6240. The bolometric luminosity estimated from the SED is $L_{24\,\mu\mathrm{m-UV}} = 2.86 \times 10^{11}\,L_{\odot}$. The stellar mass and star formation rate (SFR) of the host galaxy, derived from the fit to the u band to 4.5 μm photometry (to avoid the wavelengths where the AGN contribution can be relevant) using a set of 11 models with smooth star formation histories (Bruzual & Charlot 2003; IMF from Chabrier 2003), are $M_{\mathrm{star}} \sim 2.5 \times 10^{10}\,M_{\odot}$ and SFR $\sim 100\,M_{\odot}$ yr^{-1} (Bolzonella et al. 2009). Our estimated M_{star} and SFR are meant to be upper limits because the nuclear component can still contribute to the said quantities. Given this mass and SFR, CID-42 is actively star forming, with an SFR consistent with the overall X-ray selected AGN population (Silverman et al. 2009).

The five-year optical and near-IR light curve, as computed by Salvato et al. (2009), is shown in Figure 2 (top right). No significant variability has been detected, as expected, given that the optical SED is dominated by the host galaxy light.

The source was imaged in the X-rays for 74 ks by *XMM-Newton* and for 165 ks by *Chandra* ACIS-I. The *XMM-Newton* data were taken over 2.5 yr (eight observations) and the *Chandra* data over 1.5 yr (six observations), for a total of 14 observations over four years. The reported exposure is the sum of all the effective exposure times. The luminosities derived in the two co-added sets of observations are $L_{0.5-10\,\mathrm{keV}} = 4.8 \times 10^{43}$ erg s^{-1} and 1.9×10^{43} erg s^{-1} for *XMM-Newton* and *Chandra*, respectively. The factor of 2.5 difference between the two luminosities is too large to be explained by cross-calibration problems between the two instruments and implies significant X-ray variability. The full four-year X-ray light curve (Figure 2, right middle) shows a factor of 3 variability in the full (0.5–10 keV) band flux, while in the soft (0.5–2 keV) and hard (2–10 keV) bands the variability reaches a factor 4 and 4.5, respectively. No significant variability in the spectral slope has been measured (Figure 2, right bottom).

3. IMAGING ANALYSIS

3.1. HST Imaging Analysis

Figure 3 (left) shows a 9″ × 9″ zoom around source CID-42 in the ACS/*HST* image (0.″03 pixel^{-1}; filter F814W). The distance measured between the two optical centers is 0.″495 ± 0.″005 (16.5 pixels) which corresponds to a projected separation of 2.46 ± 0.02 kpc at the source's redshift.

We modeled the optical surface brightness of CID-42 with GALFIT (Peng et al. 2002; Version 3.0[23]). We use an empirical point-spread function (PSF) created by averaging stars in the ACS frames (Jahnke et al. 2004, 2009b) to represent a point source in the field and to use for the convolution of the parametric galaxy models.

We tested several combinations and numbers of point sources and Sersic profiles (Sersic 1968) with a free Sersic-parameter n.

[23] C. Y. Peng, 2009 private communication.

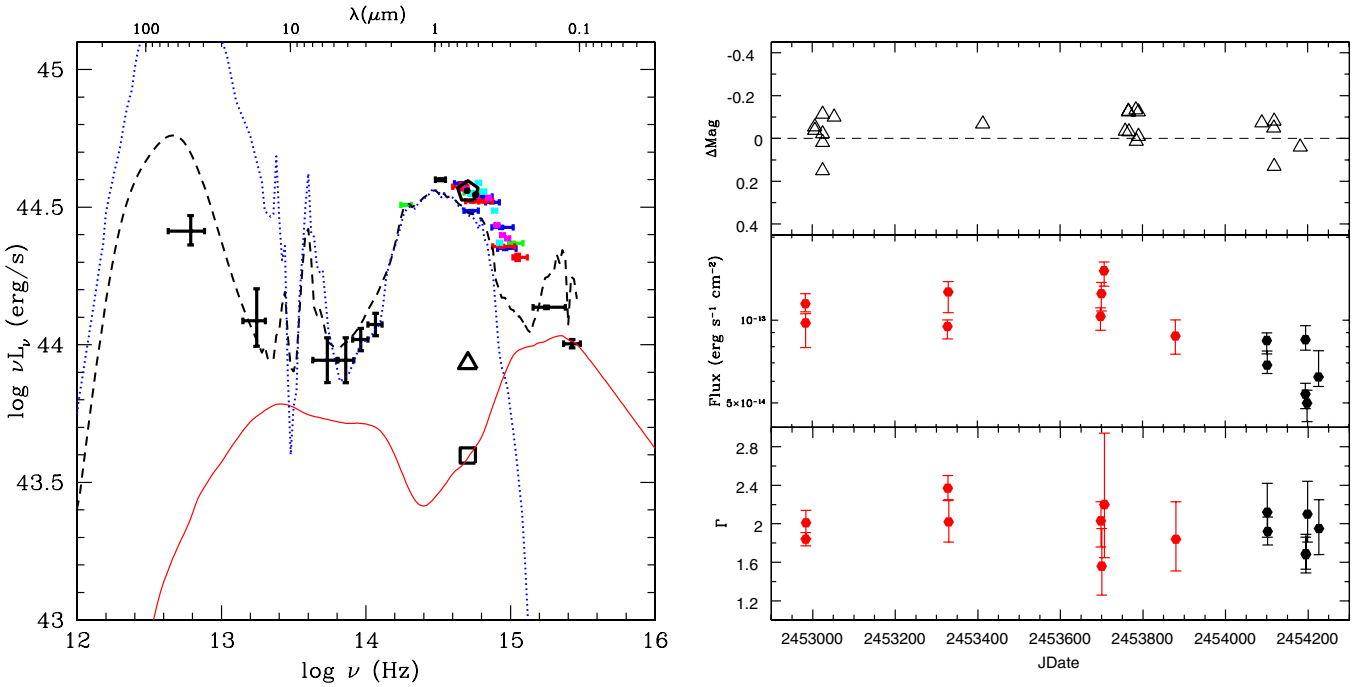

Figure 2. Left: infrared to UV rest-frame SED. The small points represent all the COSMOS data for source CID-42 with 1σ errors: MIPS 70 and 24 μm; IRAC; Canada–France–Hawaii Telescope *K*, *J*, and *i*; Subaru broad and narrow bands; SDSS; CFHT *u*; and *Galaxy Evolution Explorer*. The big symbols represent the luminosity computed for the two compact sources separately (square = SE source, triangle = NW source) and for the total system (pentagon symbol) using the surface brightness decomposition technique (Section 3). The Elvis et al. (1994) radio-quiet quasar SED (continuous red line) has been normalized to the ACS luminosity (λ5900 in the rest frame) of the SE source. The dashed and dotted lines are a Seyfert 1.8 and NGC 6240, respectively (Polletta et al. 2007). Right: top: time variability of the optical flux (as computed by Salvato et al. 2009). In the optical, CID-42 was observed during four epochs (Subaru broad band, CFHT *i* band, the first set of intermediate Subaru bands, and the second epoch of intermediate Subaru bands). Center: X-ray full band light curve (red = *XMM-Newton*, black = *Chandra*). Bottom: X-ray spectral slope vs. time.

(A color version of this figure is available in the online journal.)

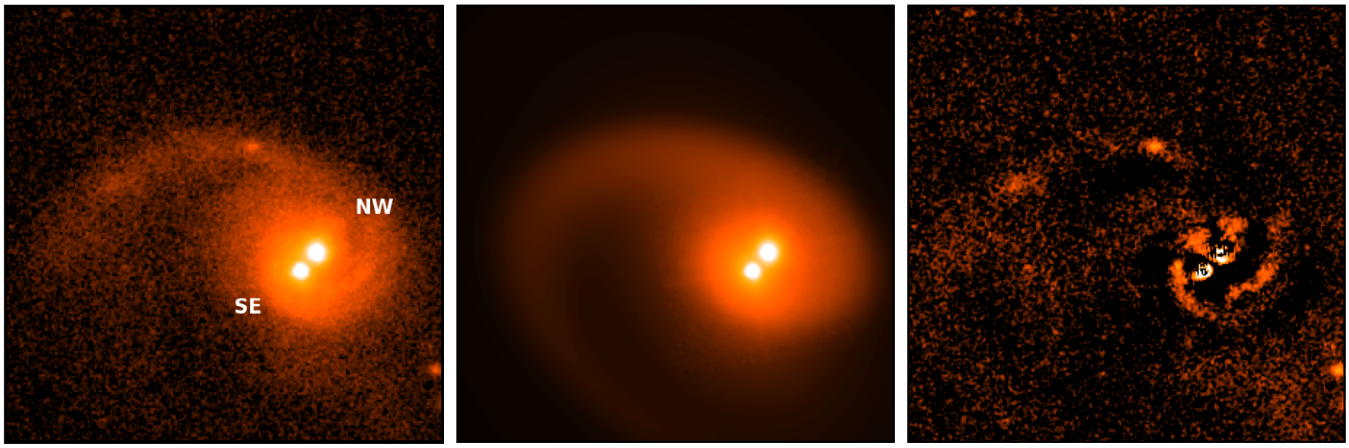

Figure 3. Surface brightness decomposition results: input 9″× 9″ACS image (left), model used (one point-like, three Sersic components; middle), and residuals obtained from the fitting (right). The images are shown in a logarithmic scale. North is up, east is to the left.

(A color version of this figure is available in the online journal.)

We also made use of two new features in GALFIT V3.0, a Fourier mode modification of isophotes, restricted in this case to F1 (lopsidedness); and a mode to model the NE tidal arm. The goals of this exercise were to (1) test whether the two nuclei in the system are point sources, (2) extract reliable point source fluxes, and (3) put constraints on the relative fluxes of the galaxy components around the two sources.

The best description of the system consists of one point source and three Sersic components. The model and the residuals are shown in Figure 3 (middle and right). We find that, above the general background, only the southeastern (SE) nucleus is well modeled with a point source, while the northwestern (NW) nucleus is extended though compact. This finding is independent of the exact number and geometry of large-scale galaxy components added to the model. By this model, we estimate the point-like SE nucleus to have F814W = 20.51 mag (square in Figure 2, left) with an uncertainty of ∼0.1 mag. The first Sersic component corresponds to the NW nucleus and is very compact, with a scale length of ∼0.″1 (∼0.5 kpc), smaller than the typical dimension of host galaxies of X-ray selected AGNs (e.g., Schade et al. 2000), and F814W = 19.67 mag (triangle in Figure 2, left). The second Sersic

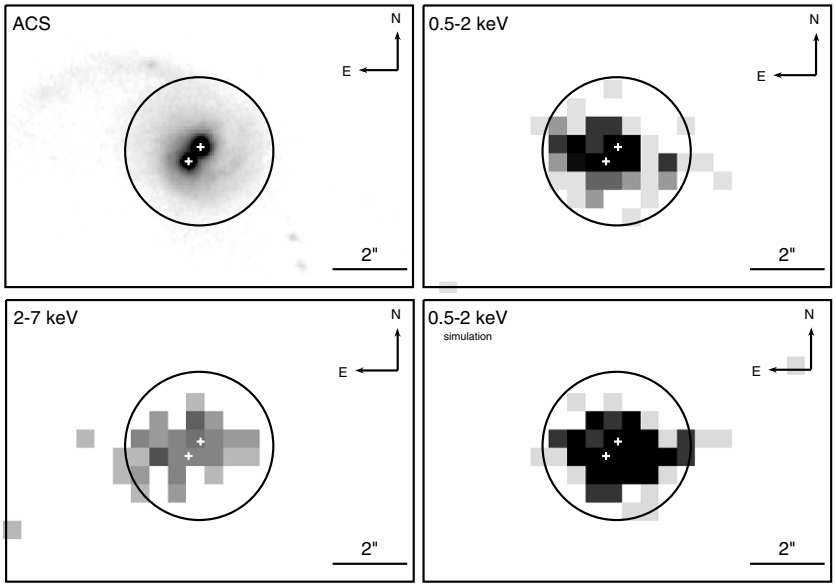

Figure 4. From top left to bottom right: *HST*/ACS image, ACIS-I images in the 0.5–2 keV, 2–7 keV energy bins, and simulated image in the 0.5–2 keV band assuming point-like emission from the two nuclei. The four images are matched on the same coordinate scale. The crosses represent the position of the optical nuclei, and the circles show a 2″radius to help in comparing the images.

component is a large spheroid ($r_{\rm eff} = 3''$, ∼15 kpc) and the third Sersic component describes part of the overall light distribution plus the spiral arm. The latter two components combined have F814W = 18.6 mag and together describe the host galaxy light distribution, likely extending the profile of the NW source. The overall system brightness obtained with the fit is F814W = 18.11 mag (pentagon in Figure 2, left), in agreement with the photometry used for the SED.

In order to test the goodness of the fit, we ran the GALFIT analysis with a simple model (one point-like source and one Sersic component), as was reported by Gabor et al. (2009). This fitting runs into calculation boundaries, indicating that a two-component model is not adequate to represent this complex system. A minimum of three components (one PSF and two Sersic) are required; the best fit is obtained using four components, as explained above.

Given the point-like unresolved profile of the SE source, it could be considered as an unobscured BH (i.e., Type 1 AGN) and it is possible to compute its bolometric luminosity by normalizing to its F814W magnitude a typical Type 1 AGN SED (Elvis et al. 1994; red line in Figure 2, left). This gives a bolometric luminosity for the SE source of $L_{24\,\mu{\rm m}-{\rm UV}} = 2.8 \times 10^{44}$ erg s^{-1}, consistent with being a moderately luminous AGN.

3.2. XMM-Newton Imaging Analysis

The merging system CID-42 is not an isolated source, as is evident in Figure 1. Using combined *XMM-Newton* and *Chandra* data (with prior point source removal), extended emission has been detected around CID-42. The X-ray detected group (Finoguenov et al. 2007; A. Finoguenov et al. 2010, in preparation) is spectroscopically confirmed with 7 galaxy members in the zCOSMOS bright catalog (Lilly et al. 2007, 2009) and 30 members in the photometric redshift catalog (Ilbert et al. 2009), of which 10 are visible in Figure 1. The extended X-ray luminosity in the 0.1–2.4 keV band is 1.4×10^{42} erg s^{-1}. The X-ray centroid, though uncertain (30″positional error), is consistent with the position of CID-42. The detection of extended X-ray emission from the hot gas of the group allows us to estimate the mass of the halo in which the merging galaxy resides. The total gravitational mass of the group is $M_{200} = (2.5 \pm 0.7) \times 10^{13}\ M_{\odot}$,[24] based on the average L_x–M_{200} calibration of Leauthaud et al. (2010). The corresponding R_{200} is 106″(∼0.5 Mpc), so CID-42 is located in the core of the group. The source CID-42 has also been identified as the second most massive group galaxy (MMGG; details in Leauthaud et al. 2010). Furthermore, the galaxy group hosting CID-42 is embedded in a large over-dense region at $z \sim 0.37$ covering the whole COSMOS field (Scoville et al. 2007b, Gilli et al. 2009).

3.3. Chandra Imaging Analysis

CID-42 was imaged with *Chandra* in six ACIS-I pointings with different exposure times (14–46 ks) and off-axis angles (3′–7.′5) spread over four months. Given the *Chandra* ACIS-I resolution (0.″5 pixel^{-1}), it is not possible to perform an accurate decomposition analysis as performed with *HST*/ACS data, but it is possible to study the emission in different energy bands.

We analyzed the X-ray emission in both soft (0.5–2 keV) and hard (2–7 keV) band images, using the observation in which the source has been observed at the smallest off-axis angle (∼3′) and with the longest exposure time (46 ks). In this observation, the source has 187 net counts in the full band in a region corresponding to 95% of the encircled energy fraction for a point source at that position.

Most of the counts (123 out of 187) are detected in the 0.5–2 keV band. Comparing to the PSF that applies to this energy band, off-axis angle, and azimuth, there is some evidence for extension along the axis joining the two optical nuclei. To characterize this better, we did a detailed ray-trace simulation using ChaRT[25] and MARX[26] with the assumption of equal flux from the two optical nuclei. The results are illustrated in Figure 4 where we show the *Chandra* soft band X-ray image (top right)

[24] M_{200} is the mass enclosed in R_{200}, which is the radius within which the matter density is 200 times the critical density of the universe.
[25] http://cxc.harvard.edu/chart/
[26] http://space.mit.edu/CXC/MARX/

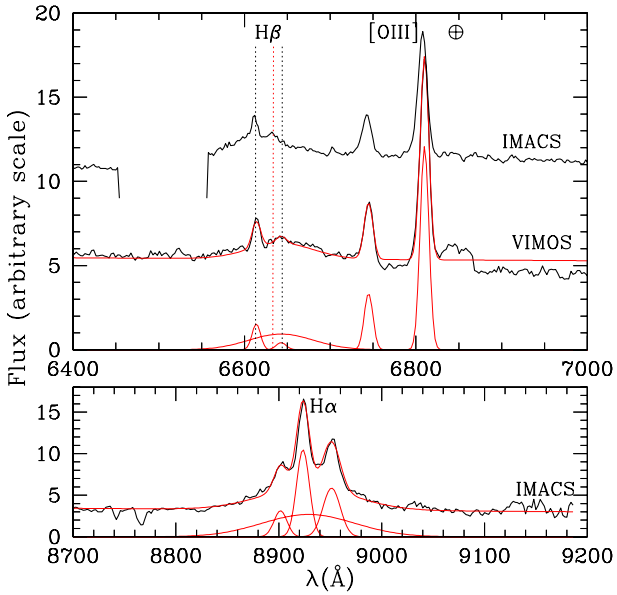

Figure 5. Top: CID-42 zCOSMOS and IMACS spectra (black line) around the Hβ line plotted in the observed frame. The components used to reproduce the spectral features in the zCOSMOS spectrum are shown at the bottom of the frame in red, as well as the spectral fit. The flux is in arbitrary unit. The emission lines used in the fit are labeled. The chip gap in the IMACS spectrum is evident. The thin dashed lines represent the observed wavelength of the zCOSMOS Hβ lines (black) and the predicted wavelength where the broad Hβ should peak in the IMACS spectrum (red). The strong residuals at 6825 Å are due to the presence of an absorption telluric line. Bottom: CID-42 IMACS spectrum around the Hα line plotted in the observed frame. The line colors are as above.

(A color version of this figure is available in the online journal.)

and the simulation (lower right). The observed and simulated images are qualitatively consistent, indicating that there is no evidence for galaxy-scale X-ray diffuse emission in this source. One would like to constrain usefully the flux ratio of the two point sources, but this is not possible here given the PSF extent and astrometric uncertainty at 3′off-axis. For completeness, we also simulated the 2–7 keV hard band data as coming from the two nuclear point sources and also in this case we found that the observed image (Figure 4, lower left) is consistent with the simulated image.

4. SPECTROSCOPIC ANALYSIS

4.1. Optical Spectroscopy

Optical spectra are available from SDSS (Adelman-McCarthy et al. 2008), IMACS/Magellan (Trump et al. 2007, 2009a), and VIMOS/VLT (zCOSMOS; Lilly et al. 2007, 2009). The source has been observed on 2005 February with IMACS and then twice with VIMOS on 2005 May and June. Given the 1″width of the slits (oriented N–S) both in the VIMOS and IMACS observations, and the small E–W separation of the sources (∼0.″3), the flux from both falls within the slit. The two-dimensional (2D) spectra have been analyzed, but none of them spatially resolve the two nuclei, while in Comerford et al. (2009) the two nuclei seem to be resolved in a 2D DEIMOS spectrum; the spatial resolution of the DEIMOS spectrum is similar to the IMACS one (IMACS: 1 pixel = 0.11″, DEIMOS: 1 pixel = 0.11″, VIMOS: 1 pixel = 0.″205) but its spectral resolution ($R \sim 3000$) is higher. The two zCOSMOS spectra (5500–9500 Å) have an average S/N of 6 (11 around the Hβ line; Figure 5) and a spectral resolution of $R \sim 600$. The IMACS spectrum (5600–9200 Å, $R \sim 700$) has a detector chip gap at 6450–6560 Å, cutting off part of the Hβ line. The Hα emission line is in a region where fringing becomes strong in VIMOS. Although Hα is visible in the IMACS spectrum, which uses the nod and shuffle techniques to avoid fringing, the peak of the line is saturated. The SDSS spectrum (4000–9000 Å) has an S/N of ∼6 around the interesting emission lines, lower than the Very Large Telescope (VLT) and Magellan spectra. The SDSS spectrum uses a 3″ fiber instead of a 1″ wide slit, and so the spectrum contains more extended emission diluting the AGN continuum.

For these reasons, we started the spectral analysis by fitting the blue part of the zCOSMOS spectrum around the Hβ and the [O III] doublet. The fitting was performed using the IRAF routine SPECFIT (Kriss 1994). We modeled the spectrum with a linear component for the continuum plus four Gaussian lines, one broad and three narrow: the [O III] doublets, and the broad and narrow Hβ. The central wavelength, width, and intensity of the Gaussians were left free to vary. The redshift measured from the peak of the narrow emission lines ([O III] and Hβ) is $z = 0.359$, coincident with the redshift listed in Lilly et al. (2007, 2009) and Comerford et al. (2009). This redshift is also consistent with the one measured from absorption lines (e.g., Hγ). The FWHM of the narrow emission lines, corrected for instrumental broadening, is 560 ± 120 km s^{-1}.

The three optical spectra show a typical Type 1.5 (Osterbrock & Ferland 2006) AGN feature: a broad Hβ component plus a narrow core that has a line width similar to the forbidden [O III] lines. Unusually though, the broad and narrow Hβ components of CID-42 have widely offset peaks, potentially implying that the emission comes from different regions, consistent with the presence of two unresolved sources. The same offset is measured in both the zCOSMOS spectra and so, in order to have a better measurement of this offset, we summed them. We measure an offset $\Delta\lambda \sim 30 \pm 7$ Å (1360 ± 320 km s^{-1}) between the centroids of the broad and narrow Hβ. Small residuals at the peak of the broad line possibly suggest the presence of another narrow component at the same wavelength that, when fitted, unfortunately has a flux below the S/N of the spectrum.

If the offset between the two components is due to the narrow lines being produced by one of the two optical sources and the broad line by the other source, then an instrumental shift due to the spatial separation and the orientation of the sources with respect to the E–W VIMOS dispersion axis has to be considered. This effect shifts the broad component toward the red by 4 Å, which should be subtracted from the measured offset. The net offset (26 ± 7 Å) implies a difference in velocity of ∼1180 ± 320 km s^{-1} between the Hβ narrow and broad components under this assumption.

The 2D IMACS spectrum (see Figure 6) shows a clear shift of the peak of the broad line with respect to the narrow line, but does not show the spatial separation seen in Comerford et al. (2009), despite the same pixel scale of the two instruments (IMACS and DEIMOS); this is most likely due to different seeing conditions.

The presence of a detector chip gap close to the Hβ region in the IMACS spectrum prevents a good fitting of the line profile. However, a narrow line is present with a broad peak redshifted from the narrow core. Using the shift measured in the zCOSMOS spectrum, we predicted the wavelength where the broad line in IMACS should peak. The instrumental shift due to position and slit orientation in the IMACS spectrum would move the broad component toward the blue (i.e., in the direction opposite to the zCOSMOS spectrum shift) because

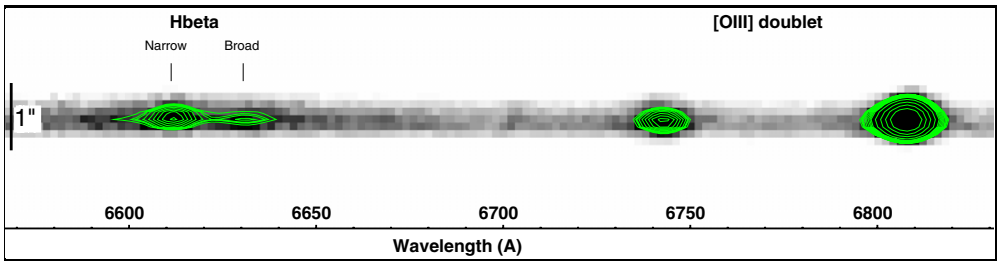

Figure 6. Two-dimensional IMACS spectrum of source CID-42: zoom around Hβ and [O III] doublet region. The contours have been produced using SAOImage DS9 analysis tools.

(A color version of this figure is available in the online journal.)

of the opposite dispersion direction of the two instruments, so that the two peaks have a different observed offset with respect to zCOSMOS. The predicted offset in IMACS is ∼20 Å, which matches with the observed line peak (red dashed line in Figure 5, top). If the lines are not coming from two different sources, the predicted offset in IMACS would not correspond with the observed line peak, although it could be consistent within the errors.

We analyzed the SDSS spectrum to check for the presence of the offsetted Hβ line, but, given the lower S/N and the higher flux of the continuum, the broad component of the Hβ line is barely above the noise in the spectrum and so we do not use it for our analysis.

We performed further checks to test the possible presence of a second system of lines with the same offset of the broad Hβ. The first would be the detection of a second [O III] doublet with the same shift measured in the Hβ but, at the expected wavelength, a Telluric feature (∼6825 Å) prevents the detection of the corresponding redshifted [O III] lines. The second test would be the detection of a redshifted broad Hα line. As explained above, Hα lies in a region dominated by fringing in the zCOSMOS spectrum, while in IMACS the line peak is saturated. The fit of the Hα and [N II] doublet in the IMACS spectrum returns three narrow lines at the same redshift of the narrow [O III] doublet (Figure 5, bottom). The broad Hα component peak is slightly offset (∼5 Å) to the red from the narrow one but this shift is not enough to be consistent with the shift predicted from Hβ, even when the instrumental shift is taken into account. Although proper fitting of the continuum has been performed, a 1:2 ratio for the [N II] doublet flux is observed instead of the 1:3 ratio required by atomic physics. On the contrary, the expected 1:3 ratio has been measured in the [O III] doublet flux in all spectra. This suggests that, around Hα, the IMACS spectrum is not well behaved and so the measurement of the broad-line peak is still uncertain.

We also performed a simple two-component fit to the IMACS spectrum to determine the relative nuclear and host contributions in the 4000–9000 Å range. Following Trump et al. (2009b), we find the combination of quasar (Vanden Berk et al. 2001) and galaxy (Eisenstein et al. 2001) that maximizes the Bayesian probability function and best describes the spectrum. The estimated nuclear-to-host ratio is ∼3:2. Systematic errors, arising from neglecting the contribution from other components, could affect this estimated ratio. However, this simple fit shows that the spectrum is not consistent with a simple blue quasar but instead includes a significant host contribution (consistent with the GALFIT decomposition of Section 3.1). The significant host contribution may also be part of the reason for which the fitting around the Hα region returns different results from those obtained for Hβ and [O III].

Table 1
Joint *XMM-Newton* pn and *Chandra* ACIS X-ray Spectral Analysis Results

Fit Parameter	*Chandra*	*XMM-Newton*
Continuum		
Mekal kT (keV)	<0.13	<0.13
Mekal $F_{0.3-2}$ (erg s^{-1} cm^{-2})	$<1.2 \times 10^{-15}$	$6.4 \times 10^{-15}\ ^{+5.2}_{-2.3}$
Photon Index Γ	$1.95^{+0.07}_{-0.06}$	$1.95^{+0.07}_{-0.06}$
$N_{\rm H}$ (10^{22} cm^{-2})	<0.02	<0.02
Emission Line		
Obs. Energy (keV)	$6.44^{+0.07}_{-0.07}$	$6.60^{+0.15}_{-0.12}$
Line σ (keV)	<0.57	<0.20
Flux (erg s^{-1} cm^{-2})	$1.50 \times 10^{-15}\ ^{+1.14}_{-0.75}$	$1.35 \times 10^{-15}\ ^{+0.90}_{-0.70}$
EW (eV)	570 ± 260	142^{+143}_{-86}
Absorption Line		
Obs. Energy (keV)	$5.86^{+0.27}_{-0.14}$	$6.01^{+0.28}_{-0.14}$
Line σ (keV)	<0.50	$0.22^{+0.33}_{-0.11}$
Flux (erg s^{-1} cm^{-2})	$-5.68 \times 10^{-16}\ ^{+4.76}_{-3.36}$	$-4.07 \times 10^{-15}\ ^{+2.23}_{-1.93}$
EW (eV)	$-200\ ^{+98}_{-95}$	$-441\ ^{+150}_{-148}$
Flux and Luminosity (erg cm^{-2} s^{-1})		
Total $F_{0.5-10}$	$4.49 \times 10^{-14}\ ^{+0.30}_{-0.20}$	$10.90 \times 10^{-14}\ ^{+1.20}_{-0.52}$
Total $L_{0.5-10}$	1.93×10^{43}	4.85×10^{43}
Total $F_{0.5-2}$	$1.89 \times 10^{-14}\ ^{+0.15}_{-0.10}$	$4.80 \times 10^{-14}\ ^{+0.34}_{-0.25}$
Total $L_{0.5-2}$	7.90×10^{42}	2.18×10^{43}
Total F_{2-10}	$2.60 \times 10^{-14}\ ^{+0.25}_{-0.20}$	$6.10 \times 10^{-14}\ ^{+0.44}_{-0.35}$
Total L_{2-10}	1.14×10^{43}	2.66×10^{43}

Note. 2σ errors are reported for all the quantities except for the EW of the lines for which we report 1σ errors.

4.2. X-ray Spectral Analysis

The X-ray data available (∼800 counts in *Chandra* ACIS and ∼2200 counts in the *XMM-Newton* pn) allow us to perform good quality X-ray spectral analysis when *XMM-Newton* pn and *Chandra* ACIS spectra are fitted together. The results are reported in Table 1. Due to the modest number of counts, we used the Cash statistic (Cash 1979). A fit with an absorbed power law returns a spectral index $\Gamma = 2.11 \pm 0.06$, with no cold intrinsic absorption, in good agreement with the results of Mainieri et al. (2007; $\Gamma = 2.18 \pm 0.07$). Residuals in the very soft energy band (<0.5 keV, mostly in the *XMM-Newton* spectrum) suggest the presence of a thermal component ($kT < 0.13$ keV) that accounts for 8%–9% of the 0.3–2 keV luminosity, which could be due to either a nuclear soft-excess or hot gas in the galaxy. The addition of the soft component to the fit produces a slightly flatter spectral slope with $\Gamma = 1.95^{+0.07}_{-0.06}$.

The most striking features of the X-ray spectrum are around 4.5 keV (observed frame; Figure 7, left). The residuals suggest the presence of both emission and absorption features in both spectra, forming a kind of *inverted* P-Cygni profile, i.e., the

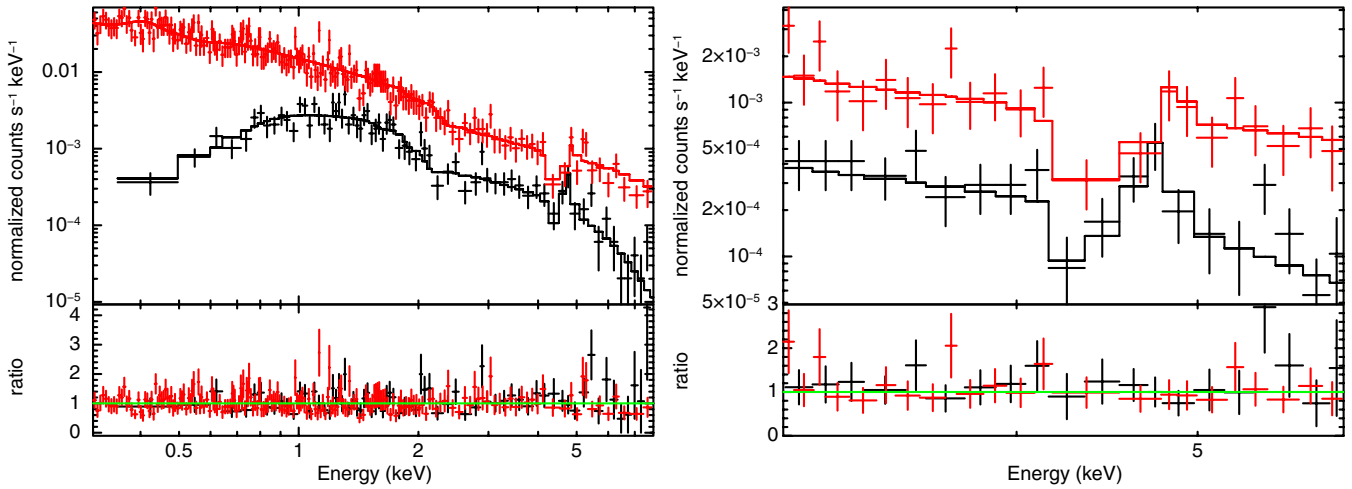

Figure 7. Left: X-ray spectra of CID-42 (*XMM-Newton* = red, *Chandra* = black) fitted with an absorbed power law plus two Gaussian lines. The spectra have been rebinned for presentation purposes at 5 counts per bin. The spectra are folded with the instrumental response. Right: zoom of the X-ray spectra at the energies around the absorption and emission features fitted with a broad and a narrow Gaussian line, respectively. The *inverted* P-Cygni profile is visible.

(A color version of this figure is available in the online journal.)

absorption component is *redshifted* with respect to the emission component (Figure 7, right).

The emission feature, which is consistent with being a neutral iron line, has a constant flux and is more prominent in the *Chandra* spectrum (EW = 570 ± 260 eV, in the rest frame), where the continuum is fainter, than in the *XMM-Newton* one (EW = 142^{+143}_{-86} eV, in the rest frame), where the continuum is 2 times higher.

The absorption feature instead shows strong variability between *XMM-Newton* and *Chandra* data, both in flux and width: the line is well fitted with a broad ($\sigma = 0.22^{+0.33}_{-0.11}$ keV, 1σ error) Gaussian line in the *XMM-Newton* spectrum, where it is more prominent, while it is unresolved in the *Chandra* data ($\sigma < 0.5$ keV). Assuming $z = 0.359$, the central rest-frame energy of the absorption line is around 6 keV, and therefore it seems to be a *redshifted* absorption iron line.

The shape and intensity of the background spectrum have been studied in order to discard the possibility for the absorption line to be a background artifact. The fact that the absorption line has been detected in spectra from two different instruments (EPIC and ACIS), already rejects this hypothesis.

In order to check if the *inverted* P-Cygni feature can be mimicked by other spectral models, we also performed the spectral fitting using more complex models—a broken power law and a partial covering model. The two models reproduce the continuum better than a single power law, given the larger number of parameters, but none of them reproduces the absorption and emission features. In particular, the edge around 5–6 keV in the partial covering model does not reproduce the absorption feature. The ΔCash statistic obtained by adding the two Gaussian lines to the models is the same as that obtained with a single power law, meaning that the absorption feature is real and independent of the model adopted to reproduce the continuum. We note that the partial covering model returns $N_{\rm H} \sim 10^{23}$ cm^{-2} and a covering fraction of 40%, which can be translated as the sum of two power laws of almost the same intensity, one obscured and the other not.

A spectral fitting with a photoionized gas model to the total *XMM-Newton* spectrum has also been performed. Unfortunately, given the low CCD resolution, it is not possible to distinguish single absorption lines in the soft band. The equivalent width of the absorption feature with a photoionized-gas model implies a high column density of the absorber ($N_{\rm H} \sim 5 \times 10^{23}$ cm^{-2}); and the modest absorption measured in the soft band ($N_{\rm H} < 0.9 \times 10^{20}$ cm^{-2} in the rest frame) requires the absorber to be highly ionized ($\log \xi \sim 3$). From the centroid of the line, we measure the velocity of the outflow of 30,000 ± 4000 km s^{-1}.

In order to check the nature of the broadening of the absorption line, we analyzed the spectra individually. Given that the *XMM-Newton* data come from eight observations taken over three years, variability may be responsible for the broadening. Nine (five *XMM-Newton* and four *Chandra*) out of the fourteen available observations have enough counts (>125) to perform an individual spectral fit. The absorption feature is present at 2σ–3σ in all the spectra, apart from one *Chandra* observation where, although the number of counts is enough for fitting (187 net counts), the continuum flux is faint and thus the absorption line is not detected. The intensity (with 1σ error), width, and rest-frame energy centroid of the line measured in the eight spectra are plotted in Figure 8 (red = *XMM-Newton*, black = *Chandra*). In contrast to the summed spectrum, the absorption features show a narrow profile, with only upper limits on the width in all the spectra ($\sigma < 250$ eV) and the EW is consistent with being constant, implying a column density of gas of $\sim 5 \times 10^{23}$ cm^{-2} (Bianchi et al. 2005).

The line energy centroid in the *XMM-Newton* spectra changes in time over the range 5.9–6.3 keV, while in the *Chandra* spectra it is almost the same, within the errors. This variation explains the broadening measured in the total *XMM-Newton* spectrum as due to the superposition of narrow lines with different energy centroids. The variability of the energy centroid is of $\Delta E = +500$ eV in the first two years and $\Delta E = -400$ eV in the last year. These shifts are comparable to the 400 eV separation of the Fe I and the Fe XXVI Kα absorption lines, so a change in ionization could, in principle, be responsible for the observed shifts. We analyzed the hardness ratio in all the spectra to check for column density variability to be related with variability of the ionization state, but, given the large error bars, we do not detect statistically relevant variability.

Instead, if this variation is converted in a pure velocity variation, it implies a range in velocity of 0.02*c*–0.07*c* for

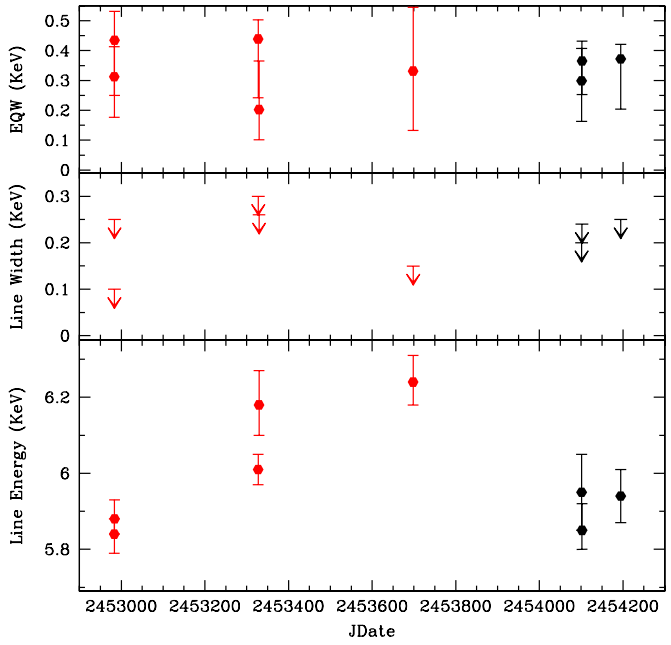

Figure 8. Absorption line parameters (equivalent width, width, and rest-frame energy of the absorption line) measured in different epochs spectra. Red symbols represent *XMM-Newton* observations (years 2003, 2004, and 2005), black symbols represent *Chandra* observations (years 2006 and 2007). Error bars on the EW are at 1σ.

(A color version of this figure is available in the online journal.)

neutral iron (Fe I), with a deceleration of 10,000 km s^{-1} yr^{-1} in the first two years and a faster acceleration in the last year of observations. If the lines are due to completely ionized iron (Fe XXVI) absorption, the velocity is higher (0.09–0.14c) and the implied acceleration is slightly lower.

Because of the degeneracy between velocity and ionization state, the same conclusions on the absorber parameters (density, ionization state, and velocity) are obtained doing the single-line analysis and the fitting with a photoionized model.

5. DISCUSSION

We report in this paper the properties of a peculiar and unique source at $z = 0.359$, CID-42, in a survey of X-ray sources with ACS counterparts in COSMOS. CID-42 is a unique source in three specific ways.

First, in the 2 deg^2 COSMOS area, there are ∼4 X-ray sources out of ∼550 at $z < 0.8$ with optical morphologies indicative of ongoing major mergers, but only one of them (CID-42) clearly shows two cores resolved in the *HST* image embedded in the same galaxy but unresolved in X-rays. The surface brightness decomposition applied to the ACS image strongly suggests the presence of a point-like unresolved source (SE source) and a more extended, but still compact, source (NW source). The tidal tails to the NE and SW, in the ACS image, are evidence of merging (Toomre & Toomre 1972; Dubinski et al. 1999; Springel & White 1999). The morphology is consistent with either an early passage state, in a phase subsequent to the first passage, or with a later stage of the merging after the coalescence of the two BHs (Mihos & Hernquist 1996; Cox et al. 2006; Hopkins et al. 2008).

Second, in three optical spectra obtained with two different instruments (VIMOS and IMACS), a velocity offset larger than 1000 km s^{-1} is measured between the broad and narrow components of the Hβ line. Large velocity offsets between two different line systems can be observed if two BHs in a virialized system are rapidly rotating very close to each other (sub-parsec separation), as suggested for the double-line system of Boroson & Lauer (2009). However, assuming that the broad and narrow lines are coming from the SE and NW sources, respectively, virialization is not appropriate for the kiloparsec-scale separation of the two sources in CID-42.

A possibility to justify the large velocity offset is a recoil effect. Large recoiling velocity have been predicted by theoretical models and simulations for both GW wave kicks (Campanelli et al. 2007a, b) and slingshot effect kicks in triple BH systems (Hoffman & Loeb 2007). The unresolved morphology of the SE source allows us to assume that it plays the role of the unobscured SMBH (a Type 1 AGN) and produces the broad Hβ line. Therefore, the SE source is recoiling with respect to the system with a velocity of >1000 km s^{-1}.

As the BH recoils from the center of a galaxy or from another BH, the closest, most tightly bound regions (disk and broad-line regions, BLRs) are carried with it, and the more distant regions (narrow-line regions, NLRs) are left behind (Merritt et al. 2006; Loeb 2007). Given the distance between the recoiling BH and the center of the whole system (measured on the plane of the sky) and one component of the BH velocity (the radial velocity) with respect to the galaxy, it is possible to compute a lower limit on the time since the BH has been kicked of $\sim 4 \times 10^6$ yr.

The detection of a recoiling BH is related to its lifetime and it is extremely rare because it never gets a large enough separation before fading. The lifetime of the active phase of the BH depends on the amount of accreting material it carries after the kick. In principle, higher velocities result in a smaller ejected disc. In CID-42, the BH is still emitting enough radiation to ionize the BLR, so it had to carry enough material in order to be still active.

It is possible to compute the BH mass of the SE source using the Vestergaard & Peterson (2006) relation between the line width, the BH mass, and the continuum luminosity, and using the Hβ line width (3500 ± 233 km s^{-1}). As shown in Figure 2, the total continuum luminosity is mostly dominated by the galaxy light. Taking advantage of the surface brightness decomposition results, we can extrapolate the 5100 Å nuclear luminosity of $\sim 4 \times 10^{43}$ erg s^{-1} by normalizing a standard quasar template (red line in Figure 2; Elvis et al. 1994) to the SE source luminosity in the ACS filter (square in Figure 2). Under this assumption, the BH mass of the SE source is $\sim 6.5 \times 10^7\ M_\odot$.

Given the total mass of the galaxy and the estimated BH mass, the ratio $M_{\rm BH}/M_\star$ is a factor 2 higher than the Häring & Rix (2004) $M_{\rm BH}$–$M_\star$ relation for local spheroids. Although the errors on the BH and galaxy mass are quite large, this is consistent with the fact that CID-42 is a peculiar source or that the local relation deviates at high z (see, for example, Treu et al. 2007 and Merloni et al. 2010). If we consider that the galaxy mass is an upper limit to the bulge mass, the offset from the relation could be even bigger. Using the bolometric luminosity and BH mass of the SE source, we find that the Eddington ratio is $L/L_{\rm Edd} \sim 0.04$, consistent with either the nuclear activity of this source having just been triggered or already declining. Using the correlation between the Eddington ratio and the bolometric correction in the 2–10 keV energy range (Vasudevan & Fabian 2009; Young et al. 2010), it is possible to estimate the 2–10 keV luminosity emitted by the SE source to be in the range $(0.6–1) \times 10^{43}$ erg s^{-1}, consistent with the 2–10 keV luminosity measured for CID-42 (see Table 1).

The third feature that makes CID-42 unique is the detection, in the X-ray spectra, of an extraordinarily strong, *redshifted*

absorption iron line and an emission iron line, forming an *inverted* P-Cygni profile. Out of the 100 X-ray sources with more than 1000 counts in the stacked X-ray spectrum only, CID-42 shows an iron line in absorption (Mainieri et al. 2007; G. Lanzuisi et al. 2010, in preparation). The absorption line is intrinsically narrow. Its energy centroid changes by 500 eV over the four years of observations. The broadening of the absorption line in the total *XMM-Newton* spectrum is the result of the stacking of narrow lines redshifted by different velocities in the different observations. Such *redshifted* absorption lines are rare. Most known X-ray absorbers in AGNs are blueshifted (see Cappi 2006 for a review) and 85% of them are at low redshift ($z < 0.2$). As blueshifted absorbers necessarily imply outflowing winds, redshifted absorbers would seem to require high-velocity inflows, which must therefore be situated very close to the central BH. The few convincing cases of redshifted lines are all narrow absorption lines detected in Seyfert 1 sources (Mrk 335, Longinotti et al. 2007; PG 1211+143, Reeves et al. 2005; Mrk 509, Dadina et al. 2005), and have suggested the explanation of gas falling with relativistic velocity directly into the BH at a few tens of gravitational radii.

The cluster of rare features seen in this source, more likely associated with a brief moment of the merging event, is a strong argument against the chance superposition hypothesis. Any model for the system should preferably link these unique features. We describe two possible models below.

5.1. GW Recoiling BH

The spatial offset of the SE point-like source with respect to the NW source and the kinematic offset of the broad Hβ line with respect to the narrow line system can be explained by an SMBH ejected by gravitational radiation produced in the BH merger.

According to theoretical models, during the final coalescence of two BHs in a merger event, the GWs produced can impart a large kick to the resultant BH, which recoils in the opposite direction with respect to the center of the galaxy (Peres 1962). Although some approximate methods indicated that the kick velocities are most likely small ($<$few $\times$ 100 km s^{-1}; Blanchet et al. 2005; Damour & Gopakumar 2006), the results from full numerical relativity simulations show that the recoil speed can be up to 4000 km s^{-1} (Campanelli et al. 2007a, 2007b).

It is difficult to estimate how often significant recoil kicks occur because the recoil kick distribution depends on the spin and mass ratio distributions of the progenitor BH binaries, which are not well known. Several authors (Schnittman & Buonanno 2007; Campanelli et al. 2007a, 2007b; and Baker et al. 2008) have estimated, using results from full numerical relativity simulations, that 12%–36% of recoiling BHs will have velocities $>$500 km s^{-1} and 3%–13% will have velocities $>$1000 km s^{-1}, assuming a spin of 0.9 with random orientations and using different assumptions on how the kick velocity scales with BH progenitor mass ratio ($0.1 < q < 1$). These fractions might be smaller if BH spins are on average lower or if gas torques are efficient at aligning the spin axes in a way that is unfavorable for large kicks (Bogdanović et al. 2007; Dotti et al. 2010). To constrain the actual recoil kick distribution, better observational constraints on merging BHs or observations of individual recoiling BHs are required. A candidate recoiling SMBH with a large kick velocity of 2650 km s^{-1} has been spectroscopically discovered by Komossa et al. (2008), although alternative models have been proposed to explain the two systems of lines in the optical spectrum. A second possible candidate has also been proposed by Shields et al. (2009).

The high-velocity offset ($v > 1000$ km s^{-1}) measured in the optical spectra of CID-42 is consistent with the numbers obtained in simulations, although the probability of finding such high-velocity recoiling BH is low ($<$10%).

The surface brightness decomposition of the CID-42 ACS image is consistent with the ejected BH hypothesis, too: the SE point-like source, the ejected BH, is spatially separated from the compact, but not point-like, NW bright source, which can easily represent the galaxy core from which the BH has been ejected.

The fact that the broad lines are redshifted with respect to the stellar absorption lines is consistent with the recoiling BH picture because they are following the BH, as explained at the beginning of Section 5, while the NLRs are left at the center of the NW source. The narrow lines have the same redshift of the stellar absorption lines but, given that the BH is more than 2.5 kpc away, the NLRs are no longer powered by it. Another way to produce the narrow lines is needed. The line flux ratios indicate that the emission is produced by nuclear activity and not by star formation (Comerford et al. 2009). The narrow lines could be produced by the ejected BH, ionizing the local galaxy ISM on its way out from the center. In this case, the narrow lines should have the same redshift of the galaxy, as observed, implying that the BH is still inside a region of the galaxy disk with high ISM density or is passing by molecular clouds. In this case, the velocity offset measured in the optical spectrum, not corrected for instrumental shift (see Section 4.1), is 1360 $\pm$ 320 km s^{-1}, which represents the radial component of the total velocity.

Lousto et al. (2010) showed, in a statistical study of BH binaries during the inspiral and merger, that when the kick velocity is $\gtrsim$1000 km s^{-1} the direction of the kick is most likely perpendicular to the BH orbital plane. They found a probability of 6.3% for large recoil velocities ($>$1000 km s^{-1}) along the line of sight. If the accretion disk is aligned with the nearly face-on galaxy disk as a whole, then a large kick closely aligned with the line of sight is expected, and it is consistent with that observed in CID-42, if the source is a recoiling BH.

The time since the BH has been kicked ($\sim 4 \times 10^6$ yr), as computed at the beginning of Section 5, is in agreement with the prediction of the effective time for the persistence of off-center quasar activity ($10^{6.2}$–10^7 yr; Blecha & Loeb 2008). This number is a lower limit but it should be a good estimate, assuming that the total kick velocity is not much higher than the radial velocity, given that this is already in the extreme tail of the kick velocity distribution predicted by models and simulations. According to the Blecha & Loeb (2008) model, for a kick velocity in the range 1100–1500 km s^{-1} and a BH mass of 10^7–10^8 $M_\odot$, the mass of the BH disc, in order to be still emitting, is $\sim$2%–3% of the BH mass.

Models predict that the effect on galaxy morphology of BH recoil is to produce significant asymmetry (Kornreich & Lovelace 2008). This is seen in the morphology of CID-42 where the galaxy core (the NW source) is slightly misplaced with respect to the geometric center of the galaxy disc.

The variable Fe–K absorption line can be alternatively explained, as already explained at the beginning of this section, by material inflowing into the BH, as it has been proposed in a few other sources (Cappi 2006; see Section 5). In order to have such a high velocity, the inflow of material would have to be very close to the nucleus (few tens of Schwarzschild radii). One way of achieving high inflow velocity is with a photon

bubble instability (Arons 1992; Gammie 1998; Begelman 2006) which produces a propagating pattern of low- and high-density regions through which the radiation has to go. The photon bubble instability is currently used to explain the *inverted* P-Cygni profiles detected in the spectra of luminous blue variable (LBV) stars (e.g., van Marle et al. 2008). Although this would be a physical explanation, it requires super-Eddington accretion, which is not observed in CID-42.

Although the high-velocity inflow possibility is very interesting, without detailed modeling it remains a mere hypothesis.

5.2. A Type 1 AGN Recoiling from a Type 2 AGN in a Slingshot

In the following, we list the evidences in favor of a picture in which CID-42 contains two AGNs, an unobscured Type 1 AGN in the SE source, and an obscured Type 2 AGN in the NW one.

1. The surface brightness decomposition of the ACS image finds a compact, but not point-like, bright source in the NW nucleus.
2. The shift ($\Delta v \sim 1180 \pm 360$ km s^{-1}) between the broad and narrow components of the Hβ line in the optical spectrum also suggests the presence of two active nuclei, one responsible for the broad-line emission (i.e., a Type 1 AGN), the other responsible for the narrow emission lines only (i.e., a Type 2 AGN). A possible explanation for the presence of only one narrow emission-line system could be that the NLRs of the two sources are mixed up and, for this reason, are at the same redshift measured for the galaxy from the absorption lines. However, we discard this hypothesis as NLRs, at the luminosity of CID-42, are expected to extend 0.1–1 kpc from the nucleus (Schmitt et al. 2003), much less than the projected separation measured between CID-42 nuclei.
3. The X-ray flux variability and the presence of a strong iron emission line (EW $\sim$ 500 eV) when the continuum is weak also suggest a combination of a variable Type 1 AGN and a constant obscured Type 2 AGN. Usually, strong iron emission lines (EW $\sim$ 1 keV) are associated with heavily obscured (Compton thick) sources and are less prominent in the unobscured ones (EW $\sim$ 150 eV; e.g., see Figure 9 of Guainazzi et al. 2005a). As already noted by Guainazzi et al. (2005b), all the AGN pairs observed so far are found to be heavily obscured or Compton thick in the X-rays, in both components. The presence of at least one obscured AGN in our system is consistent with this picture but the possibility that we have a Type 2 plus a Type 1 AGN embedded in the same galaxy is new, although we believe CID-42 is not a binary.

Assuming that the [O III] emission lines are produced by the Type 2 AGN only, it is possible to roughly estimate the contribution of the two sources to the total X-ray luminosity. The Type 2 luminosity is estimated from the relation between the $L_{2-10\,\mathrm{keV}}$–$L_{[\mathrm{O\,III}]}$ measured in the COSMOS field (Silverman et al. 2009) and the Type 1 AGN luminosity is then found by subtraction. Given the [O III] luminosity ($\sim 3 \times 10^{41}$ erg s^{-1}) and the uncertainties on this relation, the luminosity of the NW Type 2 nucleus would be $\sim 9 \times 10^{42}$ erg s^{-1} in the 2–10 keV band (not absorption corrected). The derived Type 1 AGN luminosity (2–10 keV) is in the range (0.3–1.8) $\times 10^{43}$ erg s^{-1} due to the strong measured variability (Figure 2, right). The last number is consistent with the 2–10 keV luminosity obtained in the previous section with the Eddington ratio.

As explained at the beginning of Section 5, the large velocity shift between the two nuclei implied by the optical spectra would require a large mass of the system, assuming it is virialized (i.e., the two nuclei are gravitationally bound in a circular orbit). Comerford et al. (2009) detected two sets of [O III] and Hα lines in a Keck/DEIMOS spectrum,[27] from which a $\Delta v = 150$ km s^{-1} is measured by detecting two sets of emission lines. This lower velocity shift allows a more "reasonable" mass for a virialized system; however, virialization, which is a fair assumption for close pairs, is probably not appropriate for the kiloparsec-scale separation of the two CID-42 sources. Most likely, the velocity measured by Comerford et al. (2009) is due to the rotation of the gas in the galaxy as a whole, as the system is in a violent state of gravitational interaction.

The large velocity offset between the two sources is more likely due to a nearly radial orbit, with the Type 1 SE AGN recoiling with respect to the Type 2 AGN. A velocity difference of this size may result from a slingshot ejection in a triple BH encounter (Saslaw et al. 1974; Hoffman & Loeb 2006, 2007). If a BH binary stalls for a $\sim$few Gyr before it coalesces, due to the depletion of stars in the loss cone in a gas-poor merger (Merritt & Milosavljević 2005), its host galaxy could merge with another galaxy and a third BH may spiral in and undergo a strong three-body interaction with the binary. The system that just arrived will merge with the original galaxy. The SFR ($\sim 100\,M_\odot$ yr^{-1}) measured from the SED fitting supports the scenario of a merger in an early phase. The merger will drive mass and gas to the binary, refilling its loss cone. The configuration will become gravitationally unstable and this event will end with the further reduction of the separation or the coalescence of the binary and the ejection of the lightest body at a speed comparable to the binary's orbital speed (Heggie 1975).

The large projected distance (2.4 kpc) between the two sources and the high velocity measured in CID-42 are possible for this kind of ejection (Hoffman & Loeb 2006, 2007), although the probability to have a certain velocity at a certain separation depends from the initial condition of the system. Given that all massive galaxies have possibly experienced a merger event in the last ten billion years, assuming uncorrelated events, and a typical binary lifetime of one billion years, then 10% of SMBH binaries may form a triplet. However, even though the triple interaction would possibly lead to an ejection of one or even all SMBHs (Valtonen et al. 1994), most of the triple systems live long ($\sim 10^9$ yr; Hoffman & Loeb 2007), and final coalescence is more common (85% versus 15%) than ejection.

5.2.1. Backlit Wind Model

On the basis of the above analysis, the SE nucleus is the unobscured Type 1 recoiling AGN, while the NW is an obscured Type 2 AGN resulting from the coalescence of a binary. The two nuclei lie close to the plane of the sky possibly moving in a radial orbit in a direction close to the line of sight, though a small angle has to be considered given the 2.4 kpc separation. Relative to the mean velocity of the system, the SE nucleus is moving away from the observer and the NW one toward the observer. The suggested geometry of the system is shown in Figure 9.

The SE Type 1 nucleus then has (1) a strong unobscured optical continuum, leading to the point-like *HST*/ACS image; (2) the broad Hβ emission line; and (3) a strong, variable,

[27] Although the spectral resolution of the Comerford et al. (2009) spectrum is higher than that of the IMACS and VLT spectra one, the S/N, estimated from their Figure 3, is lower.

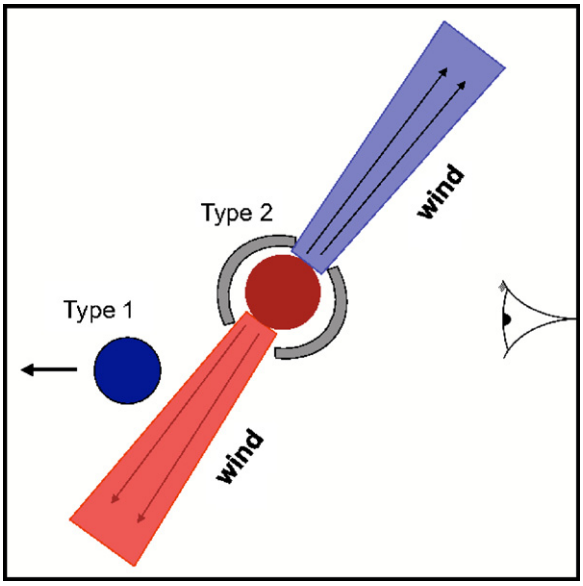

Figure 9. Backlit Wind model sketch. The proposed geometry for the system is presented. In red, the Type 2 AGN (NW nucleus) with the absorbing material around (gray); in blue, the Type 1 (SE nucleus). The component of the BAL-like wind, which block the line of sight toward the Type 1 AGN, is shown as a red cone. The blueshifted wind (blue cone) is unobservable. The line of sight is presented with a symbolic eye.

(A color version of this figure is available in the online journal.)

X-ray continuum emission. The obscured NW Type 2 nucleus has (1) a weak optical continuum, leading to a compact but extended *HST*/ACS source dominated by the galaxy light; (2) only narrow emission lines of Hβ and [O III]; and (3) a weak X-ray continuum, with a strong fluorescent iron emission line (EW $\geqslant$ 570 eV).

However, the high-velocity infall scenario could still be a possible interpretation of the Fe–K absorption line (see Section 5.1); the proximity of the two sources allows special interpretation as a "Backlit Wind." In this scenario, a fast, highly ionized BAL-like wind is emitted by the NW Type 2 nucleus (located in front). In almost all circumstances, this wind would be undetectable. However, in the case of CID-42, the *receding* wind crosses our line of sight to the SE Type 1 nucleus, leading to absorption of the Type 1 continuum in redshifted iron. The blueshifted emission of the approaching wind remains invisible as there is no background source to illuminate it. The column density of the flow derived from the EW of the absorption line is consistent with what is seen in BAL wind ($>10^{23}$ cm^{-2}; Green et al. 2001; Gallagher et al. 2002; Chartas et al. 2009). The fact that we measure no X-ray photoelectric absorption at low energies implies that the wind is highly ionized, something also observed in other BAL (e.g., Telfer et al. 1998; Hamann 1998; Chartas et al. 2009) and X-ray absorbers (e.g., Vignali et al. 2000; Reeves et al. 2009).

The variations of the iron absorption line energy centroid on a timescale of years can be explained either by velocity variations ($\sim$10,000 km s^{-1} per year) in the flow, or by a change in the ionization state, and so in the density (Proga et al. 2000), or, possibly, to a precession of the flow, so that a change in inclination can produce a difference in velocity, or by a combination of all these effects. BALs, when we look directly along the flow, are known to vary on year timescales (e.g., Lundgren et al. 2007; Gibson et al. 2008), so variability should be more likely in a section viewed across the flow. The variability implies that the BAL-like flow must be highly structured, even 2.5 kpc away from the nucleus. This is not unusual as it has been shown by *Chandra* detection of radio jets still relativistic at megaparsec distance from their origin (e.g., PKS 0637-752; Schwartz et al. 2000).

As we have only one example of a *redshifted* iron absorber and only one recoiling BH, this scenario is only plausible if the BAL-like wind has a large opening angle, making an interception of the rear recoiling Type 1 nucleus likely.

Winds at a few 1000 km s^{-1} are normal in Type 1 AGNs (Reynolds 1997; Piconcelli et al. 2005) and much faster (0.1c–0.2c) BAL winds, confined to modest solid angles, are not unusual (Weymann et al. 1991; Hamann et al. 1993; Ogle et al. 2000). Fast winds at kiloparsec-scale distances from Type 1 AGNs have been found as well (Arav et al. 2001) and have been proposed to be universal in AGNs (Elvis 2000). However, there has been no possibility to test this idea in Type 2 AGNs. CID-42 provides this opportunity and gives us the first detection of a wind in a Type 2 AGN.

6. CONCLUSIONS

We have reported the multiwavelength properties of CID-42, which shows three unusual features: two close sources embedded in the same galaxy, resolved in the optical ACS image, but unresolved in the X-ray one; a high-velocity offset, measured between the broad and narrow Hβ lines in three different optical spectra; and a *redshifted* absorption iron line in the X-ray spectrum.

Thanks to the rich database of the COSMOS survey, the analysis of the properties of CID-42 has been performed at all wavelengths.

The overall analysis suggests two possible explanations for the source: a GW recoiling BH, caught a $\sim$few megayears after the kick from the center of the galaxy or a Type 1/Type 2 AGN system where the Type 1 is recoiling due to a slingshot effect.

Analysis of the ACS image shows the presence of an SE point-like source, playing the role of the Type 1 AGN (or SMBH with disc and BLRs) in both scenarios, confirmed by the X-ray flux variability across time and by the offset in velocity measured between the narrow and the broad components of the Hβ line. The NW source, being less compact than the SE one, could be either the naked core of the galaxy from which a BH has been kicked out or a Type 2 AGN.

The presence of a *redshifted* absorption iron line changing its energy centroid in the different observations allows us to explain the geometry of the system by inflow of material into the BH in the GW recoil BH case or with the "Backlit Wind" model in the second scenario. Monitoring observations in the X-ray would be suitable to study the moving X-ray absorption feature and its variability.

The "Backlit Wind" implies that fast BAL-like winds are present in Type 2 AGNs, an otherwise untestable hypothesis. The variability of the iron absorption is, in this special case, a new tool to study BAL flows. This model predicts corresponding high-ionization UV absorption lines (e.g., O VI), making CID-42 a suitable target for *HST*/COS observations. *Chandra* high-resolution observations with the High Resolution Camera could resolve the two sources to see if both are X-ray emitting or not, while optical and IR spectroscopy with higher spatial resolution, which is currently only possible with *HST*, could confirm the still uncertain velocity shift measured in Hβ in other lines.

If future observations allow us to confirm that the GW recoiling BH is the best explanation of the system, it will be

the first time that this phenomenon is observed via both a spatial offset from the galactic core and a velocity offset in the optical spectrum.

Although models for this system have been sketched qualitatively in this paper, a numerical analysis will be the subject of a forthcoming paper.

Upcoming Keck Integral Field Unit (IFU) observations with OSIRIS will help us to disentangle major competing models mapping the inner region of CID-42. IFU observations on larger scales could map the velocity of gases and stars in the galaxy and in the tails in order to constrain the theoretical models on the geometry of the merger and the inclination of the galaxies in the first encounter (D'Onghia et al. in preparation).

Calibrating the number of recoiling BH, produced either in close triple encounters or by GW ejection, could be of great importance for the proposed *Laser Interferometer Space Antenna* (*LISA*) mission (see discussion in Loeb 2010).

CID-42 is a unique source with a cluster of rare features. The presence of a dual AGN has also been proposed for this source on the basis of a Keck spectrum (Comerford et al. 2009) and has not yet been disproved. Whichever is the best explanation, in CID-42 we are possibly witnessing a runaway BH.

F.C. thanks E. Costantini, T. J. Cox, M. Dotti, L. Hernquist, and A. Sesana for useful discussion. The authors thank Chien Y. Peng for useful discussions about GALFIT. The authors thank the anonymous referee, whose critical analysis helped improve this paper, making it more interesting. This work was supported in part by NASA *Chandra* grant number GO7-8136A (F.C., M.E., and A.F.), NASA contract NAS8-39073 (Chandra X-ray Center). K.J. acknowledges support from the Emmy Noether Programme of the German Science Foundation (DFG) through grant number JA 1114/3-1. In Italy, this work is supported by ASI/INAF contracts I/023/05/0, I/024/05/0, and I/088/06, and by PRIN/MUR grant 2006-02-5203. In Germany, this project is supported by the Bundesministerium für Bildung und Forschung/Deutsches Zentrum für Luft und Raumfahrt and the Max Planck Society.

Facilities: CXO (ACIS), *HST* (ACS), *XMM* (pn)

REFERENCES

Adelman-McCarthy, J. K., et al. 2008, ApJS, 175, 297
Arav, N., et al. 2001, ApJ, 561, 118
Arons, J. 1992, ApJ, 388, 561
Baker, J. G., Boggs, W. D., Centrella, J., Kelly, B. J., McWilliams, S. T., Miller, M. C., & van Meter, J. R. 2008, ApJ, 682, L29
Ballo, L., Braito, V., Della Ceca, R., Maraschi, L., Tavecchio, F., & Dadina, M. 2004, ApJ, 600, 634
Begelman, M. C. 2006, ApJ, 643, 1065
Bekenstein, J. D. 1973, ApJ, 183, 657
Bianchi, S., Chiaberge, M., Piconcelli, E., Guainazzi, M., & Matt, G. 2008, MNRAS, 386, 105
Bianchi, S., Matt, G., Nicastro, F., Porquet, D., & Dubau, J. 2005, MNRAS, 357, 599
Blanchet, L., Qusailah, M. S. S., & Will, C. M. 2005, ApJ, 635, 508
Blecha, L., & Loeb, A. 2008, MNRAS, 390, 1311
Bogdanović, T., Reynolds, C. S., & Miller, M. C. 2007, ApJ, 661, L147
Bolzonella, M., et al. 2009, arXiv:0907.0013
Bondi, M., Ciliegi, P., Schinnerer, E., Smolčić, V., Jahnke, K., Carilli, C., & Zamorani, G. 2008, ApJ, 681, 1129
Bonning, E. W., Shields, G. A., & Salviander, S. 2007, ApJ, 666, L13
Boroson, T. A., & Lauer, T. R. 2009, Nature, 458, 53
Brandt, W. N., & Hasinger, G. 2005, ARA&A, 43, 827
Brusa, M., et al. 2007, ApJS, 172, 353
Brusa, M., et al. 2010, ApJ, in press (arXiv:1004.2790)
Bruzual, G., & Charlot, S. 2003, MNRAS, 344, 1000
Campanelli, M., Lousto, C. O., Zlochower, Y., & Merritt, D. 2007a, Phys. Rev. Lett., 98, 231102
Campanelli, M., Lousto, C., Zlochower, Y., & Merritt, D. 2007b, ApJ, 659, L5
Capak, P., et al. 2007, ApJS, 172, 99
Cappelluti, N., et al. 2009, A&A, 497, 635
Cappi, M. 2006, Astronom. Nachr., 327, 1012
Cash 1979, ApJ, 228, 939
Chabrier, G. 2003, PASP, 115, 763
Chartas, G., Saez, C., Brandt, W. N., Giustini, M., & Garmire, G. P. 2009, ApJ, 706, 644
Chornock, R., et al. 2010, ApJ, 709, L39
Colpi, M., & Dotti, M. 2009, arXiv:0906.4339
Comerford, J. M., Griffith, R. L., Gerke, B. F., Cooper, M. C., Newman, J. A., Davis, M., & Stern, D. 2009, ApJ, 702, L82
Cox, T. J., Jonsson, P., Primack, J. R., & Somerville, R. S. 2006, MNRAS, 373, 1013
Dadina, M., Cappi, M., Malaguti, G., Ponti, G., & de Rosa, A. 2005, A&A, 442, 461
Damour, T., & Gopakumar, A. 2006, Phys. Rev. D, 73, 124006
Dotti, M., Volonteri, M., Perego, A., Colpi, M., Ruszkowski, M., & Haardt, F. 2010, MNRAS, 402, 682
Dubinski, J., Mihos, J. C., & Hernquist, L. 1999, ApJ, 526, 607
Eisenstein, D. J., et al. 2001, AJ, 122, 2267
Elvis, M. 2000, ApJ, 545, 63
Elvis, M. 2009, BAAS, 41, 708
Elvis, M., et al. 1994, ApJS, 95, 1
Elvis, M., et al. 2009, ApJS, 184, 158
Finoguenov, A., et al. 2007, ApJS, 172, 182
Frayer, D. T., et al. 2009, AJ, 138, 1261
Gabor, J. M., et al. 2009, ApJ, 691, 705
Gallagher, S. C., Brandt, W. N., Chartas, G., & Garmire, G. P. 2002, ApJ, 567, 37
Gammie, C. F. 1998, MNRAS, 297, 929
Gebhardt, K., et al. 2000, ApJ, 539, L13
Gibson, R. R., Brandt, W. N., Schneider, D. P., & Gallagher, S. C. 2008, ApJ, 675, 985
Gilli, R., et al. 2009, A&A, 494, 33
Green, P. J., Aldcroft, T. L., Mathur, S., Wilkes, B. J., & Elvis, M. 2001, ApJ, 558, 109
Guainazzi, M., Matt, G., & Perola, G. C. 2005b, A&A, 444, 119
Guainazzi, M., Piconcelli, E., Jiménez-Bailón, E., & Matt, G. 2005a, A&A, 429, L9
Hamann, F. 1998, ApJ, 500, 798
Hamann, F., Korista, K. T., & Morris, S. L. 1993, ApJ, 415, 541
Häring, N., & Rix, H.-W. 2004, ApJ, 604, L89
Hasinger, G., et al. 2007, ApJS, 172, 29
Heggie, D. C. 1975, MNRAS, 173, 729
Hoffman, L., & Loeb, A. 2006, ApJ, 638, L75
Hoffman, L., & Loeb, A. 2007, MNRAS, 377, 957
Hopkins, P. F., Hernquist, L., Cox, T. J., & Kereš, D. 2008, ApJS, 175, 356
Hudson, D. S., Reiprich, T. H., Clarke, T. E., & Sarazin, C. L. 2006, A&A, 453, 433
Ilbert, O., et al. 2009, ApJ, 690, 1236
Jahnke, K., Elbaz, D., Pantin, E., Böhm, A., Wisotzki, L., Letawe, G., Chantry, V., & Lagage, P.-O. 2009a, ApJ, 700, 1820
Jahnke, K., et al. 2004, ApJ, 614, 568
Jahnke, K., et al. 2009b, ApJ, 706, L215
Kim, M., Ho, L. C., Peng, C. Y., & Im, M. 2007, ApJ, 658, 107
Koekemoer, A. M., et al. 2007, ApJS, 172, 196
Komossa, S., Burwitz, V., Hasinger, G., Predehl, P., Kaastra, J. S., & Ikebe, Y. 2003, ApJ, 582, L15
Komossa, S., Zhou, H., & Lu, H. 2008, ApJ, 678, L81
Kornreich, D. A., & Lovelace, R. V. E. 2008, ApJ, 681, 104
Kriss, G. 1994, in ASP Conf. Ser. 61, Astronomical Data Analysis Software and Systems, ed. D. R. Crabtree, R. J. Hanisch, & J. Barnes (San Francisco, CA: ASP), 437
Leauthaud, A., et al. 2007, ApJS, 172, 219
Leauthaud, A., et al. 2010, ApJ, 709, 97
Le Floch, E., et al. 2009, ApJ, 703, 222
Lilly, S. J., et al. 2007, ApJS, 172, 70
Lilly, S. J., et al. 2009, ApJS, 184, 218
Loeb, A. 2007, Phys. Rev. Lett., 99, 041103
Loeb, A. 2010, Phys. Rev., 81, 047503
Longinotti, A. L., Sim, S. A., Nandra, K., & Cappi, M. 2007, MNRAS, 374, 237
Lousto, C. O., Nakano, H., Zlochower, Y., & Campanelli, M. 2010, Phys. Rev., 81, 084023

Lundgren, B. F., Wilhite, B. C., Brunner, R. J., Hall, P. B., Schneider, D. P., York, D. G., Vanden Berk, D. E., & Brinkmann, J. 2007, ApJ, 656, 73
Magain, P., Letawe, G., Courbin, F., Jablonka, P., Jahnke, K., Meylan, G., & Wisotzki, L. 2005, Nature, 437, 381
Magorrian, J., et al. 1998, AJ, 115, 2285
Mainieri, V., et al. 2007, ApJS, 172, 368
McCracken, H. J., et al. 2010, ApJ, 708, 202
Merloni, A., et al. 2010, ApJ, 708, 137
Merritt, D., & Milosavljević, M. 2005, Living Rev. Relativ., 8, 8
Merritt, D., Storchi-Bergmann, T., Robinson, A., Batcheldor, D., Axon, D., & Cid Fernandes, R. 2006, MNRAS, 367, 1746
Mihos, J. C., & Hernquist, L. 1996, ApJ, 464, 641
Ogle, P. M., Marshall, H. L., Lee, J. C., & Canizares, C. R. 2000, ApJ, 545, L81
Oke, J. B., & Gunn, J. E. 1983, ApJ, 266, 713
Osterbrock, D. E., & Ferland, G. J. 2006, Astrophysics of Gaseous Nebulae and Active Galactic Nuclei (2nd ed.; Sausalito, CA: Univ. Science Books)
Peng, C. Y., Ho, L. C., Impey, C. D., & Rix, H.-W. 2002, AJ, 124, 266
Peres, A. 1962, Phys. Rev., 128, 2471
Piconcelli, E., Jimenez-Bailón, E., Guainazzi, M., Schartel, N., Rodríguez-Pascual, P. M., & Santos-Lleó, M. 2005, A&A, 432, 15
Polletta, M., et al. 2007, ApJ, 663, 81
Proga, D., Stone, J. M., & Kallman, T. R. 2000, ApJ, 543, 686
Reeves, J. N., Pounds, K., Uttley, P., Kraemer, S., Mushotzky, R., Yaqoob, T., George, I. M., & Turner, T. J. 2005, ApJ, 633, L81
Reeves, J. N., et al. 2009, ApJ, 701, 493
Reynolds, C. S. 1997, MNRAS, 286, 513
Rodriguez, C., Taylor, G. B., Zavala, R. T., Peck, A. B., Pollack, L. K., & Romani, R. W. 2006, ApJ, 646, 49
Salvato, M., et al. 2009, ApJ, 690, 1250
Sanders, D. B., et al. 2007, ApJS, 172, 86
Saslaw, W. C., Valtonen, M. J., & Aarseth, S. J. 1974, ApJ, 190, 253
Schade, D. J., Boyle, B. J., & Letawsky, M. 2000, MNRAS, 315, 498
Schinnerer, E., et al. 2007, ApJS, 172, 46
Schmitt, H. R., Donley, J. L., Antonucci, R. R. J., Hutchings, J. B., Kinney, A. L., & Pringle, J. E. 2003, ApJ, 597, 768
Schnittman, J. D., & Buonanno, A. 2007, ApJ, 662, L63
Schwartz, D. A., et al. 2000, ApJ, 540, L69
Scoville, N., et al. 2007a, ApJS, 172, 1
Scoville, N., et al. 2007b, ApJS, 172, 150
Sersic, J. L. 1968, Atlas de galaxias australes (Cordoba, Argentina: Observatorio Astronomico)
Shields, G. A., et al. 2009, ApJ, 707, 936
Silverman, J. D., et al. 2009, ApJ, 696, 396
Springel, V., & White, S. D. M. 1999, MNRAS, 307, 162
Springel, V., et al. 2005, Nature, 435, 629
Taniguchi, Y., et al. 2007, ApJS, 172, 9
Telfer, R. C., Kriss, G. A., Zheng, W., Davidsen, A. F., & Green, R. F. 1998, ApJ, 509, 132
Toomre, A., & Toomre, J. 1972, ApJ, 178, 623
Treu, T., Woo, J.-H., Malkan, M. A., & Blandford, R. D. 2007, ApJ, 667, 117
Trump, J. R., et al. 2007, ApJS, 172, 383
Trump, J. R., et al. 2009a, ApJ, 696, 1195
Trump, J. R., et al. 2009b, ApJ, 706, 797
Valtonen, M. J., Mikkola, S., Heinamaki, P., & Valtonen, H. 1994, ApJS, 95, 69
van Marle, A. J., Owocki, S. P., & Shaviv, N. J. 2008, MNRAS, 389, 1353
Vanden Berk, D. E., et al. 2001, AJ, 122, 549
Vasudevan, R. V., & Fabian, A. C. 2009, MNRAS, 392, 1124
Vestergaard, M., & Peterson, B. M. 2006, ApJ, 641, 689
Vignali, C., Comastri, A., Nicastro, F., Matt, G., Fiore, F., & Palumbo, G. G. C. 2000, A&A, 362, 69
Volonteri, M., & Madau, P. 2008, ApJ, 687, L57
Volonteri, M., Miller, J. M., & Dotti, M. 2009, ApJ, 703, L86
Weymann, R. J., Morris, S. L., Foltz, C. B., & Hewett, P. C. 1991, ApJ, 373, 23
Wilkes, B. J., & Elvis, M. 1987, ApJ, 323, 243
Young, M., Elvis, M., & Risaliti, G. 2010, ApJ, 708, 1388
Zamojski, M. A., et al. 2007, ApJS, 172, 468